Journal of Alloys and Compounds 522 (2012) 114–117

Contents lists available at SciVerse ScienceDirect

Journal of Alloys and Compounds

journal homepage: www.elsevier.com/locate/jallcom

Correlation between the structural and optical properties of Mn-doped ZnO nanoparticles

Cuong Ton-That [a,*], Matthew Foley [a], Matthew R. Phillips [a], Takuya Tsuzuki [b], Zoe Smith [b]

[a] School of Physics and Advanced Materials, University of Technology Sydney, P.O. Box 123, Broadway, NSW 2007, Australia
[b] Centre for Material and Fibre Innovation, Deakin University, Pigdons Road, Geelong, VIC 3217, Australia

ARTICLE INFO

Article history:
Received 7 November 2011
Received in revised form 10 January 2012
Accepted 18 January 2012
Available online 27 January 2012

Keywords:
ZnO
Doping
Bandgap
Cathodoluminescence

ABSTRACT

The crystallographic and optical properties of Mn-doped ZnO nanoparticles prepared by a sol–gel process have been investigated by X-ray diffraction, UV-visible absorption spectroscopy and cathodoluminescence microanalysis. X-ray diffraction reveals that the nanoparticles have hexagonal wurtzite crystal structure, with the lattice constants along the *a*- and *c*-axes increasing with increasing Mn concentration from 0 to 2.4 at%. For all Mn concentrations in this range, the nanoparticles are essentially free of native point defects so that they exhibit only band-edge luminescence. The optical bandgap and band-edge emission energies for Mn-doped ZnO were found to increase in proportion to the lattice constants. The direct correlation between the bandgap and crystal structure suggests that the band-edge optical properties of Mn-doped ZnO is predominantly influenced by the amount of Mn atoms substituting Zn on the lattice sites.

1. Introduction

The possibility of bandgap engineering and influencing physical and magnetic properties by alloying wide bandgap semiconductors has provided a strong impetus to study doping effects on electronic compounds [1]. Advances in the synthesis of high-quality ZnO nanostructures are enabling device applications, in particular, light emitters with nanoscale dimensions and ferromagnetic semiconductors, yet the effect of transition metal doping on near-band-edge optical emission of ZnO is still a subject of considerable debate. Several studies have focused on Mn doping of ZnO; however, the results in the open literature are contradictory. For example, the relationship between the bandgap and Mn content has been reported to be linear [2,3], a second-order polynomial [4–6] and non-monotonic [7,8]. This makes the reproducibility of ferromagnetism in Mn-doped ZnO a challenging problem since the magnetic behaviour of the material is highly sensitive to its electronic structure [9,10].

A key issue with the growth of transition metal (TM)-doped ZnO bulk and nanocrystals is the possible existence of secondary phases [11,12], especially for specimens prepared by high temperature processes. Previous attempts of doping nanocrystals have been fraught with problems because dopants are frequently expelled to the surface by the intrinsic process of self-annealing [13]. This makes TM-doped ZnO exhibit interesting properties but also contribute to wide discrepancies in reported optical properties of ZnO nanoparticles. One way to overcome this issue is to quantify relationships between the core structure of nanoparticles and their optical data. For this purpose, we have prepared ZnO specimens doped with Mn in the concentration range from 0 to 2.4 at% and evaluated the relationship between the optical bandgap and crystal structure of the host material. It will be shown that the bandgap of Mn-doped ZnO is directly correlated with the lattice constants of the host material.

2. Experimental

2.1. Synthesis

The starting materials, $Zn(CH_3COO)_2{\cdot}2H_2O$ (Aldrich, >99.0%), Na_2CO_3 (Aldrich, >99.5%) and $Mn(CH_3COO)_2{\cdot}4H_2O$ (Aldrich, >99%) were used without further purification. The synthesis of undoped ZnO particulates was conducted via the following reaction.

$$Zn(CH_3COO)_2{\cdot}2H_2O + Na_2CO_3 \rightarrow ZnCO_3 + 2Na(CH_3COO)$$

In a typical synthesis of undoped ZnO, 13.5 g of $Zn(CH_3COO)_2{\cdot}2H_2O$ and 6.5 g of Na_2CO_3 were separately dissolved in 50 ml of deionised water. The Na_2CO_3 solution was added into the $Zn(CH_3COO)_2{\cdot}2H_2O$ solution to form white precipitates. The precipitates were separated from the supernatant using a centrifuge and further washed with deionised water to remove reaction by-products until the salinity of the supernatant becomes less than 100 ppm. The separated precipitates were dried in air at 60 °C and then heat treated at 350 °C for 1 h. For the synthesis of Mn-doped ZnO particulates, a mixture of up to 3 mol% $Mn(CH_3COO)_2{\cdot}4H_2O$ in $Zn(CH_3COO)_2{\cdot}2H_2O$ was dissolved in 50 ml of deionised water and then mixed with an aqueous solution of Na_2CO_3, followed by the same procedure as for undoped ZnO. This synthesis method resulted in ZnO nanoparticles, which undergoes an observable colour change from white to beige with increasing Mn concentration.

* Corresponding author. Tel.: +61 2 95142201; fax: +61 2 95142219.
E-mail address: Cuong.Ton-That@uts.edu.au (C. Ton-That).

0925-8388/$ – see front matter © 2012 Elsevier B.V. All rights reserved.
doi:10.1016/j.jallcom.2012.01.116

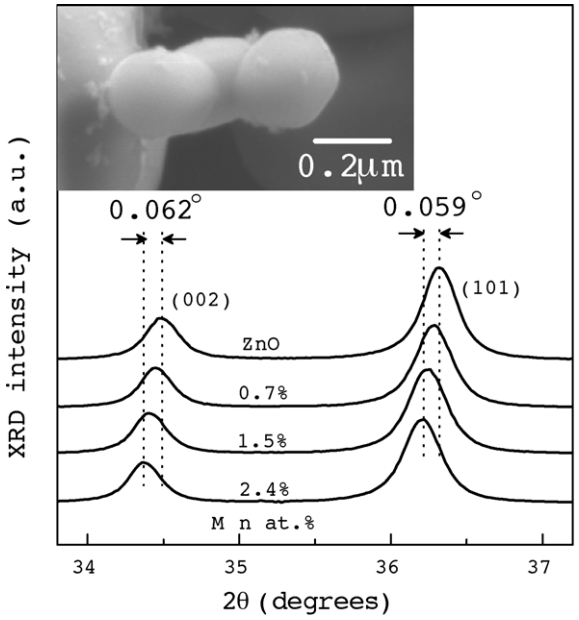

Fig. 1. XRD of pure and Mn-doped ZnO nanoparticles. Peak shifts of 0.059° and 0.062° were observed for the (1 0 1) and (0 0 2) lines of 2.4 at% Mn-doped ZnO with respect to pure ZnO. The inset shows an SEM image of ZnO nanoparticles.

2.2. Characterisation

The morphology and optical properties of the nanoparticles were investigated using a FEI QUANTA 200 scanning electron microscope (SEM) fitted with a GATAN Mono CL3 spectrometer system for cathodoluminescence (CL) measurements. The CL signal was dispersed by a 1200 lines/mm grating, collected by a parabolic mirror and detected with a Hamamatsu R943-02 Peltier cooled photomultiplier tube. All CL spectra were converted from wavelength to energy space, and corrected for the overall detection response of the CL spectroscopy system. Crystal structure identification of the particulates was determined by high-resolution X-ray diffraction (XRD) on a Siemens D5000 X-ray diffractometer using the Cu Kα radiation ($\lambda = 0.15406$ nm). For optical bandgap measurements, nanoparticles were deposited on a glass substrate. Diffuse reflectance and transmission optical data were collected using a Perkin-Elmer UV-vis spectrophotometer fitted with an integrating sphere coupled to an Oriel Cornerstone 260 1/4 m Monochromater. This setup is insensitive to directional reflection from the substrate and provides reproducible averaged response of the nanoparticles. The concentrations of Mn in the nanoparticles were measured by X-ray Photoelectron Spectroscopy (XPS), which was conducted at the Soft X-ray Spectroscopy beamline of the Australian Synchrotron.

3. Results and discussion

SEM images of pure and doped ZnO nanoparticles reveal nearly spherical shape with dimensions in the range 100–250 nm (inset, Fig. 1). XRD patterns of the pure and Mn-doped nanoparticles reveal a single hexagonal wurtzite structure, with two strong peaks ZnO (0 0 2) and (1 0 1) at approximately 34.5° and 36.3°, respectively. The presence of Mn dopants (up to 2.4 at%) does not influence the shape and crystal structure of the nanoparticles; however, XRD peak shifts are discernible. The concentration range in this study is well below the equilibrium Mn solubility limit in bulk ZnO (~12 at% [14]) to prevent surface segregation in the nanoparticles. Mn ions introduced as dopants at levels up to 2.4 at% shift the diffraction peaks to lower angles, indicating that the unit cell expands to accommodate the ions. This result is illustrated in Fig. 1, which shows peak shifts of 0.059° and 0.062° in the ZnO (1 0 1) and (0 0 2) diffraction lines, respectively, for 2.4 at% Mn-doped ZnO. Such a change is expected since Mn is known to substitutionally replace Zn in the lattice [15] and has a larger ionic radius than Zn (0.80 Å compared with 0.74 Å for the ions in the tetrahedral symmetry). This change to the unit cell dimensions is in agreement with previous observations in Mn-doped ZnO bulk [4,6] and nanostructures [16].

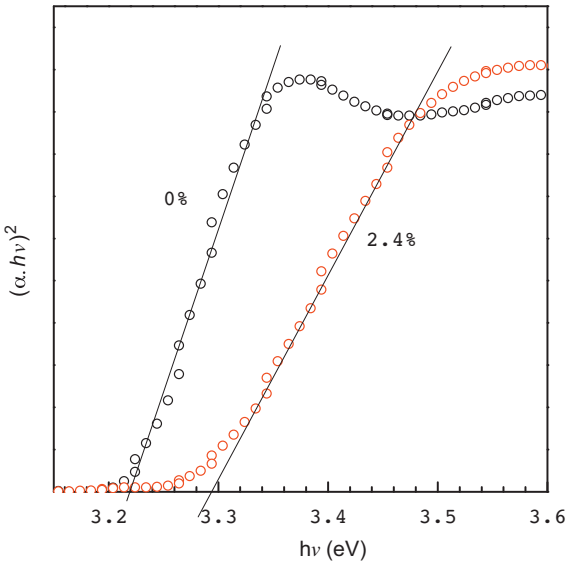

Fig. 2. Plot of $(\alpha \cdot h\nu)^2$ versus $h\nu$ for ZnO nanoparticles (see text for details). Intercept of the extrapolated lines near the absorption onset with the x-axis indicates the bandgap of 3.22 and 3.29 eV for pure and 2.4 at% Mn-doped ZnO, respectively.

The XRD peaks were fitted with Pearson VII analytical functions, yielding the angular positions. The lattice parameters (a and c) were derived based on Bragg's law and the d spacing for hexagonal crystals, which yield

$$\frac{\sin^2\theta}{\lambda^2} = \frac{h^2 + hk + k^2}{3a^2} + \frac{l^2}{4c^2}$$

where θ is the diffraction angle, ($h\,k\,l$) the Miller indices, and a and c are the lattice constants of ZnO.

Optical absorption (UV–visible) measurements reveal a clear shift in the absorption onset in nanoparticles doped with Mn. The optical bandgap was derived based on the Tauc relationship for direct bandgap semiconductors [17]:

$$\alpha = A\frac{(h\nu - E)^{1/2}}{h\nu}$$

where α is the absorption coefficient, E the bandgap and A a constant. Bandgap was obtained by extrapolating the linear region near in the absorption onset in a plot of $(\alpha \cdot h\upsilon)^2$ versus $h\upsilon$ (Fig. 2) which shows the bandgap increases from 3.22 to 3.29 eV with an increase in Mn concentration from 0 to 2.4 at%. This accords with the anticipation that the bandgap would increase with increasing Mn concentration due to the band continuum and Mn forming chemical bonding states with ZnO [3,18]. Since the size of the nanoparticles is significantly larger than the ZnO Bohr radius of 2.34 nm [19], no quantum size effects are expected. This bandgap expansion is accompanied a notable reduction in the optical transparency of the nanoparticles. The total transmittance in the visible region is greater than 80% for the undoped nanoparticles but decreases sharply to ~35% for 2.4% Mn-doped ZnO. This is due to midgap absorption, which has been attributed to the internal d–d transition of Mn ions [3].

Fig. 3 shows the normalised CL spectra of ZnO nanoparticles doped with various contents of Mn. These spectra were acquired under identical electron beam conditions (10 keV, 3.8 nA) at 80 K; under such excitation conditions the CL signal from the specimens was observed to be stable during prolonged irradiation. All nanoparticles exhibit only near-band-edge (NBE) emission. The absence of commonly observed deep-level emissions in the region of 2.1–2.5 eV, characteristic of points defects which are common with bulk ZnO [20]. This is remarkable because it suggests that the

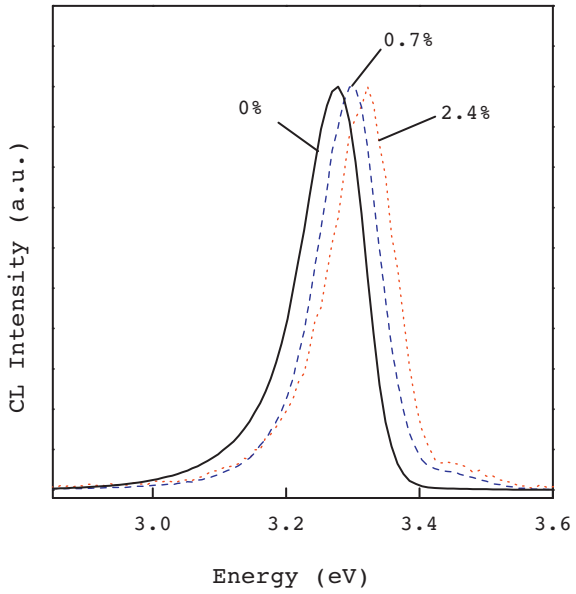

Fig. 3. Normalised CL spectra (beam energy 10 keV, current 3.8 nA, temperature 80 K) of the near-band-edge emission of ZnO nanoparticles doped with different levels of Mn, showing a blue shift with an increase in Mn concentration from 0 to 2.4 at%. (For interpretation of the references to colour in this figure legend, the reader is referred to the web version of the article.)

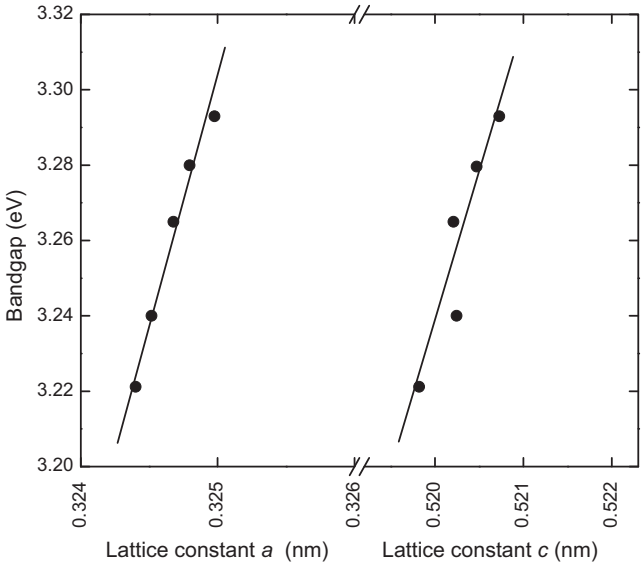

Fig. 4. Variation of the optical bandgap as a function of lattice constants *a* and *c* for Mn-doped ZnO nanoparticles, showing linear relationships with both parameters.

nanoparticles are essentially free of native point defects, despite the introduction of Mn ions. This is also indicative of the success of the doping scheme. Mn doping does not change the shape of the emission profile; however, the CL emission profile of the nanoparticles with ≥1% Mn is slightly broadened due to structural disorder induced by the substitution of Mn ions. A clear shift in the NBE emission is discernible: Mn doping blue shifts the emission from 3.25 to 3.32 eV with an increase in Mn concentration from 0 to 2.4 at%, reflecting the change in the exciton energy observed in the optical absorption measurements. The amount of the blue shift (80 meV) is the same as that of the optical bandgap. The CL intensity was found to decrease drastically with increasing Mn concentration, with the integrated intensity being reduced by more than two orders of magnitude as the Mn concentration increases from 0 to 2.4 at%. Similar quenching of luminescence has been observed previously in nanocrystals and bulk ZnO [5,21,22]. The mechanism of quenching is, however, not clear but is most likely due to the creation of a deep donor level, which provide efficient competitive channels for non-radiative recombination via the dopant Mn 3*d* levels [23].

Previously reported relationships between the bandgap and the Mn doping content have shown drastic variations from linearity [3] to non-monotonicity [7]. Such discrepancies are likely due to the fact that not all Mn ions are expected to substitute Zn ions and only a fraction of them is incorporating into the ZnO lattice. The notable differences in the effect of Mn doping suggest that the microstructure of Mn-doped ZnO and the distribution of Mn in the host material are different depending on the synthesis method and growth modes. Rutherford backscattering (RBS) measurements of sputtered Mn-doped ZnO thin films showed only 25% of Mn atoms substituting for Zn sites in the lattice while the rest was present in other forms [12]. On the other hand, the band-edge optical properties are mainly affected by the fraction of substitutional Mn ions. Although no secondary phases in the nanoparticles have been found by XRD, any Mn-rich precipitates would be too small to be detected by this technique. To elucidate the above intuitive idea, we have plotted the bandgap as a function of the lattice constants *a* and *c* (Fig. 4). A systematic increase in the bandgap with the *a*- and *c*-axis lattice constants can clearly been envisaged. We found the following empirical relationships:

$$E_g = 121.6a - 36.22\,\text{eV}$$

$$E_g = 66.36c - 31.27\,\text{eV}$$

where E_g is the bandgap energy at 300 K, *a* and *c* are in nm. The bandgap blue shifts in proportion to both lattice parameters, demonstrating a direct correlation between the crystallographic structure and the optical bandgap. This correlation also indicates that the optical bandgap is predominantly influenced by Mn ions substituting Zn on the lattice sites and thus can be considered as a measure of the Mn amount being incorporated into the ZnO host lattice. Viswanatha et al. [7] suggested that the expansion of the bandgap of Mn-doped ZnO with increasing Mn concentration was due to the presence of MnO, which is a larger bulk bandgap (4.2 eV) than that of ZnO. The correlation between the structural and optical properties, however, rules out the possibility of this superposition, but supports the continuum band model for Mn-doped ZnO [3,18]. Recently it has been shown that ferromagnetism in transition metal-doped ZnO may emerge from metallic clusters rather than ions being distributed within the host matrix [11]. Further investigations are needed to understand the ferromagnetic behaviour of the system completely.

In conclusion, we have prepared high-quality ZnO nanoparticles doped with Mn by the sol–gel technique. A systematic study of the structural and optical properties showed that the bandgap is directly correlated with the lattice parameters for Mn concentrations in the range from 0 to 2.4 at%. The bandgap is found to follow the relationships $E_g = 121.6a - 36.22$ eV and $E_g = 66.36c - 31.27$ eV, where *a* and *c* are *a*- and *c*-axis lattice constants, respectively. This correlation suggests the bandgap depends predominantly on the substitutional fraction of Mn in ZnO.

Acknowledgements

We are grateful to M. Berkahn and R. Wuhrer, both from the Microstructural Analysis Unit, for technical assistance. This work was supported by the Australian Synchrotron Research Program.

References

[1] For a review, see C. Liu, F. Yun, H. Morkoc, J. Mater. Sci. – Mater. Electron. 16 (2005) 555, and references therein.
[2] F.K. Shan, B.I. Kim, G.X. Liu, Z.F. Liu, J.Y. Sohn, W.J. Lee, B.C. Shin, Y.S. Yu, J. Appl. Phys. 95 (2004) 4772.
[3] T. Fukumura, Z.W. Jin, A. Ohtomo, H. Koinuma, M. Kawasaki, Appl. Phys. Lett. 75 (1999) 3366.
[4] A. Tiwari, C. Jin, A. Kvit, D. Kumar, J.F. Muth, J. Narayan, Solid State Commun. 121 (2002) 371.
[5] Y.S. Wang, P.J. Thomas, P. O'Brien, J. Phys. Chem. B 110 (2006) 21412.
[6] V. Avrutin, N. Izyumskaya, U. Ozgur, A. El-Shaer, H. Lee, W. Schoch, F. Reuss, V.G. Beshenkov, A.N. Pustovit, A.C. Mofor, A. Bakin, H. Morkoc, A. Waag, Superlattices Microstruct. 39 (2006) 291.
[7] R. Viswanatha, S. Sapra, S. Sen Gupta, B. Satpati, P.V. Satyam, B.N. Dev, D.D. Sarma, J. Phys. Chem. B 108 (2004) 6303.
[8] S.V. Bhat, F.L. Deepak, Solid State Commun. 135 (2005) 345.
[9] T. Dietl, H. Ohno, F. Matsukura, J. Cibert, D. Ferrand, Science 287 (2000) 1019.
[10] T. Dietl, J. Appl. Phys. 103 (2008) 07D111.
[11] K. Potzger, S.Q. Zhou, H. Reuther, A. Mucklich, F. Eichhorn, N. Schell, W. Skorupa, M. Helm, J. Fassbender, T. Herrmannsdorfer, T.P. Papageorgiou, Appl. Phys. Lett. 88 (2006) 052508.
[12] C. Liu, F. Yun, B. Xiao, S.J. Cho, Y.T. Moon, H. Morkoc, M. Abouzaid, R. Ruterana, K.M. Yu, W. Walukiewicz, J. Appl. Phys. 97 (2005) 126107.
[13] S.C. Erwin, L.J. Zu, M.I. Haftel, A.L. Efros, T.A. Kennedy, D.J. Norris, Nature 436 (2005) 91.
[14] C.H. Bates, W.B. White, R. Roy, J. Inorg. Nucl. Chem. 28 (1966) 397.
[15] Z.W. Jin, Y.Z. Yoo, T. Sekiguchi, T. Chikyow, H. Ofuchi, H. Fujioka, M. Oshima, H. Koinuma, Appl. Phys. Lett. 83 (2003) 39.
[16] M.X. Yuan, W.Y. Fu, H.B. Yang, Q.J. Yu, S.K. Liu, Q. Zhao, Y.M. Sui, D. Ma, P. Sun, Y.Y. Zhang, B.M. Luo, Mater. Lett. 63 (2009) 1574.
[17] J. Tauc, R. Grigorvici, Y. Yanca, Phys. Stat. Sol. 15 (1966) 627.
[18] X.M. Cheng, C.L. Chien, J. Appl. Phys. 93 (2003) 7876.
[19] Y. Gu, I.L. Kuskovsky, M. Yin, S. O'Brien, G.F. Neumark, Appl. Phys. Lett. 85 (2004) 3833.
[20] L.C.L. Lem, C. Ton-That, M.R. Phillips, J. Mater. Res. 26 (2011) 2912.
[21] M. Liu, A.H. Kitai, P. Mascher, J. Lumines. 54 (1992) 35.
[22] C. Ton-That, M. Foley, L. Lee Cheong Lem, G. McCredie, M.R. Phillips, B.C.C. Cowie, Mater. Lett. 64 (2010) 386.
[23] J.P. Han, P.Q. Mantas, A.M.R. Senos, J. Eur. Ceram. Soc. 22 (2002) 49.